Research Paper
Computational Methods for Differential Equations
http://cmde.tabrizu.ac.ir
Vol. *, No. *, *, pp. 1-19
DOI:10.22034/cmde.2024.62193.2725

On the wavelet Galerkin method for solving the fractional Fredholm integro-differential equations

Sharareh Ranjbari[1], Mahdi Baghmisheh[1,*], Mohammad Jahangiri Rad[1], and Behzad Nemati Saray[2]
[1]Department of Mathematics, Tabriz Branch, Islamic Azad University, Tabriz, Iran.
[2]Department of Mathematics, Institute for Advanced Studies in Basic Sciences (IASBS), Zanjan 45137-66731, Iran.

Abstract

An effective scheme is presented to estimate the numerical solution of fractional integro-differential equations (FIDEs). In the present method, to obtain the solution of the FIDEs, they must be first reduced to the corresponding Volterra-Fredholm integral equations (VFIEs) with the weakly singular kernel. Then, applying the matrix that represents the fractional integral (FI) based on biorthogonal Hermite cubic spline scaling bases (BHCSSb), and using the wavelet Galerkin method, the reduced problem can be solved. The combination of singularity and the challenge related to nonlinearity poses a formidable obstacle in solving the desired equations, but our method overcomes them well. Our investigation of the method convergence is provided, and it verifies that the convergence rate is $O(2^{-J})$ where $J \in \mathbb{N}_0$ is the refinement level. Convergence verification has also been done by presenting several numerical examples. Compared to other methods, it has been shown that the obtained results have better accuracy.

Keywords. Wavelet Galerkin method, Fractional integro-differential equation, Biorthogonal wavelet, Hermite cubic splines, Convergence analysis.
2010 Mathematics Subject Classification. 65N60, 47G20, 65T60, 65D07, 65Bxx.

1. Introduction

Integro-differential equations are frequently used in scientific applications, particularly when transforming initial or boundary value problems into integral equations. These equations also appear in modeling some phenomena, including circuit analysis, epidemiology, etc. They contain both integral and differential operators within them, in which the derivative can be of any order. It is worth noting that for obtaining the particular solution of these types of equations, the initial conditions should be given. The general η-order integro-differential equation states as

$$w^{(\eta)}(x) + \int_{\Omega} g(t, w(t))dt = f(x, w(x)), \quad w^{(\nu)}(0) = w_\nu, \quad \nu = 0, \ldots, \eta - 1.$$

where f and g are analytical functions that can be linear or non-linear.

As we know, it is generally difficult and sometimes impossible to obtain the exact solution of integro-differential equations. Meanwhile, the main goal of applied mathematics is to develop numerical algorithms to get better accuracy or find efficient algorithms.

1.1. A glance over the FIDEs.

This paper is organized to implement and develop the Galerkin method to find the numerical solution of the fractional integro-differential equations (FIDEs)

$$ {}^{C}\mathcal{D}_0^{\kappa} w(x) = c_1 f(x, w(x)) + c_2 \int_{\Omega} k(x, t) g(w(t))dt, \qquad x \in \Omega, \tag{1.1}$$

with initial conditions

$$w^{(\nu)}(0) = w_\nu, \quad \nu = 0, \ldots, \eta - 1, \tag{1.2}$$

Received: 20 June 2024 ; Accepted: 06 October 2024.
∗ Corresponding author. Email: baghmishe@iaut.ac.ir .

in which $\Omega = [0, 1]$, c_1, c_2 are constants, and ${}^{C}\mathcal{D}_0^{\kappa}$ indicates the Caputo fractional derivative (CFD) of order κ ($\kappa \in \mathbb{R}^+$) where $\eta = \kappa$ for $\kappa \in \mathbb{N}$ and $[\kappa] + 1 := \eta \in \mathbb{N}$, for $\kappa \notin \mathbb{N}$.

Furthermore, in (1.1), $f : \Omega \times \mathbb{R} \to \mathbb{R}$ is a sufficiently smooth function that can be linear or nonlinear, $k := \Omega \times \Omega \to \mathbb{R}$ is a continuous function, and the linear or nonlinear function $g : C(\Omega) \to \mathbb{R}$ fulfills the Lipschitz condition

$$|g(w_1) - g(w_2)| \leq \rho |w_1 - w_2|, \tag{1.3}$$

with Lipschitz constant $\rho > 0$.

Fractional integro-differential equations (FIDEs) (1.1) appear in modeling various physical phenomena, such as the epidemic process [3], viscoelasticity [14] and glass-forming process [2]. Numerical approaches for solving these types of equations have been considered in some papers, and we mention a few of them. In [25] authors employed the Adomian decomposition scheme to solve the FFIDEs. Then Momani et al. [26] applied this method for solving systems of FFIDEs. Rawashdeh [29], applied collocation method using Splines to solve the problem. In [4], FIDEs is solved using Fractional differential transform scheme.

Zhu et al. [38], have utilized the Galerkin method, which uses the Chebyshev wavelet, to study the specific case of Equation (1.1), i.e.,

$${}^{C}\mathcal{D}_0^{\kappa} w(x) - \int_{\Omega} k(x, t)[w(t)]^{\upsilon} dt = f(x), \quad \upsilon > 1. \tag{1.4}$$

In [38], the acting of the fractional integral (FI) operator on the Chebyshev wavelet is represented as an operational matrix, and then equation (1.4) is solved using the Galerkin method and an integration operational matrix.

Saeedi et al. [32], introduced the operational matrix of FI for the CAS wavelets and used it to solve the equation (1.4). To do this, the wavelet Galerkin method has been applied. For more study, we refer the reader to [**? ? ? ?**]

1.2. **A glance over the fractional differential equations.** In recent years, fractional differential equations (FDEs) and their applications in modeling physical phenomena have received much attention from scientists and researchers. In the literature review, the traces of these equations can be seen in many phenomena, including solid mechanics [30], anomalous transport [23], viscoelastic materials [7], fluid-dynamic traffic [16], economics [8], colored noise [20], continuum, statistical mechanics [19], nonlinear oscillation of earthquakes [15], and so on. There exist several papers that suggest techniques to find the analytical solution to such equations. But, analytical methods no longer work when the equation is complicated, so often, one can not consider them. Numerical methods are the best to overcome this issue. Among the numerical methods, we can point out some of them, such as the Adams scheme [13, 22, 34], Adomian decomposition method [24], Bernoulli wavelet method [28], finite difference method [21], polynomial interpolation [6], predictor-corrector method [10], the B-spline wavelet collocation method [18], piecewise quadratic polynomial interpolation [37], Alpert's multiwavelet method [5], and Legendre wavelet method [33].

1.3. **A glance over the multiwavelets.** Because of their properties, wavelets have been highly regarded by mathematicians in many applications, especially in solving various kinds of equations. Compared to scaler wavelets, multiwavelets have received more attention due to having various characteristics such as orthogonality, symmetry, high vanishing moment and closed form. Besides, in order to increase its vanishing moment, in contrast to Bi-orthogonal wavelets, there is no need to increase the support of these bases. Multiwavelets construct by translation and dilation of a finite number of generators such that they satisfy the vector refinement relation. Alpert's multi-wavelets [1, 35, 36] and biorthogonal Hermite cubic spline (BHCS) [11] have been drawn among the famous wavelets that have received the most attention from mathematicians in numerical analysis. BHCSSb will be introduced and discussed in detail in the second Section.

The wavelet system offers a range of useful properties that can be employed in a variety of applications. Wavelets can be used to construct operational matrices that are useful for representing a variety of operators, such as derivatives, integrals, etc. One of the key benefits of using operational matrices obtained by wavelets is that they enable sparsity, meaning that for this type of function, the number of operational matrix elements is much less compared to others. As you know, this can help reduce processing costs and make operations more efficient. Another important feature of this type of basis is that they have multi-scale properties, and this property is done with the help of the parameter J. That is, with the increase of J, the bases are refined and the approximation accuracy increases. This property can be

very useful especially when the function has a discontinuity or does not have a continuous derivative. In such cases, we choose the parameter J to be large. For large J, the error gets bounded by the fact that the interval is small.

1.4. **The main framework and goal of this paper.** In current study, we are going to implement and develop the Galerkin method to find the numerical solution of the FIDEs. The framework of this paper is as follows:

- After introducing some preliminary definitions and concepts of fractional calculus, we introduce BHCSSb in Section 2.
- Section 3 relates to implementing the Galerkin method based on BHCSSb to solve Eq. (1.1). A convergence investigation is also surveyed in this section.
- In Sect. 4, some numerical experiments are provided to show how accurate and useful the method is.
- Finally, we complete this work through the inclusion of a conclusion in section 5.

2. Preliminaries

Note that due to the importance of the topic, It is worth re-reading the preliminary concepts of fractional calculus. Due to this subject, we start this subsection with it, and then a review of BHCSSb is given along with their characteristics.

2.1. Required fractional concepts.

Definition 2.1. Given $\kappa \in \mathbb{R}^+$, the FI operator $\mathcal{I}_a^\kappa$ of order κ is specified by

$$\mathcal{I}_0^\kappa(v)(x) := \frac{1}{\Gamma(\kappa)} \int_0^x (x-z)^{\kappa-1} v(z) dz, \quad x \in [0,1], \tag{2.1}$$

where $\Gamma(\kappa)$ indicates the Gamma function.

Given the power function, its fractional integration is also a power function. That is

$$\mathcal{I}_0^\kappa(x^\alpha) = \frac{\Gamma(\alpha+1)}{\Gamma(\kappa+\alpha+1)} x^{\kappa+\alpha}. \tag{2.2}$$

It can be verified that $\mathcal{I}_0^\kappa$ can be bounded. We present the following lemma to determine this bound (cf Lemma 2.1 (a), [17]).

Lemma 2.2. *There is an estimation of the bound of the fractional integral operator $\mathcal{I}_0^\kappa$ in $L_q([0,1])$, viz*

$$\|\mathcal{I}_0^\kappa(w)\|_q \le \frac{1}{\Gamma(\kappa+1)} \|w\|_q, \quad 1 \le q \le \infty. \tag{2.3}$$

Definition 2.3. Considering $\kappa \in \mathbb{R}^+$ and $[\kappa]+1 := \eta \in \mathbb{N}$, let $\mathcal{D}^\eta := \frac{d^\eta}{dx^\eta}$. Then ${}^R\mathcal{D}_0^\kappa$ is assigned to indicate the Riemann-Liouville fractional derivative (RLFD) operator

$${}^R\mathcal{D}_0^\kappa(w)(x) := \mathcal{D}^\eta \mathcal{I}_0^{\eta-\kappa}(w)(x) = \frac{1}{\Gamma(\eta-\kappa)} \mathcal{D}^\eta \int_0^x (x-z)^{\eta-\kappa-1} w(z) dz.$$

Definition 2.4. [17] Considering $\kappa \in \mathbb{R}^+$ and $[\kappa]+1 := \eta \in \mathbb{N}$, we indicate the Caputo fractional derivative (CFD) ${}^c\mathcal{D}_0^\kappa$ as

$${}^c\mathcal{D}_0^\kappa(w)(x) := \frac{1}{\Gamma(\eta-\kappa)} \int_0^x \frac{w^{(\eta)}(z) dz}{(x-z)^{\kappa-\eta+1}} =: \mathcal{I}_0^{\eta-\kappa} \mathcal{D}^\eta(w)(x). \tag{2.4}$$

Lemma 2.5. *(cf Corollary 2.3 (a), [17]). There is an estimation of the bound of the norm of CFD operator ${}^c\mathcal{D}_0^\kappa$, viz,*

$$\|{}^c\mathcal{D}_0^\kappa(w)\|_C \le \frac{1}{\Gamma(\eta-\kappa)(\eta-\kappa+1)} \|w\|_{C^\eta}, \tag{2.5}$$

in which $\kappa \in \mathbb{R}^+$, $\kappa \notin \mathbb{N}_0$ and $\eta = -[-\kappa]$.

2.2. **Biorthogonal Hermite cubic spline scaling bases.** A brief introduction to BHCSSb will be provided in this subsection. Motivated by [11], BHCSSb consists of two piecewise functions

$$\phi^1(x) = \begin{cases} -2x^3 - 3x^2 + 1, & -1 \le x \le 0, \\ 2x^3 - 3x^2 + 1, & 0 \le x \le 1, \\ 0, & o.w, \end{cases} \tag{2.6}$$

and

$$\phi^2(x) = \begin{cases} x + 2x^2 + x^3, & -1 \le x \le 0, \\ x - 2x^2 + x^3, & 0 \le x \le 1, \\ 0, & o.w. \end{cases} \tag{2.7}$$

We note that $\phi^1, \phi^2 \in C^1(\mathbb{R})$ and fulfill the essentials of Hermite interpolation [11] as follows

$$\phi^1(\theta) = \delta_{0,\theta}, \quad \phi^2(\theta) = 0, \quad (\phi^1)'(\theta) = 0, \quad (\phi^2)'(\theta) = \delta_{0,\theta}, \quad \forall \theta \in \mathbb{Z}, \tag{2.8}$$

in which $\delta_{i,j}$ denotes the Kronecker delta.

To cover the multiresolution analysis (MRA) properties, we consider a subspace of $L_2([0,1])$ as follows

$$V_J := span\{\{\phi^k_{J,b} | b \in \mathcal{J}, k = 1, 2\} \bigcup \{\sqrt{2}\phi^1_{J,0}|_{[0,1]}, \sqrt{2}\phi^1_{J,2^J}|_{[0,1]}\}\}, \tag{2.9}$$

where $J \in \mathbb{N}_0$, $\mathcal{J} := \{1, \ldots, 2^J - 1\}$ and $\phi^k_{J,b} := \phi^k(2^J . - b)$.

It follows from MRA that the vector function $\phi = (\phi^1, \phi^2)$ has to satisfy the refinement relation, i.e.,

$$\phi(x) = \sum_{b \in \mathbb{Z}} H_k \phi(2x - b), \tag{2.10}$$

with the matrices of coefficients

$$H_{-1} = \begin{pmatrix} 1/2 & 3/4 \\ -1/8 & -1/8 \end{pmatrix}, \quad H_0 = \begin{pmatrix} 1 & 0 \\ 0 & 1/2 \end{pmatrix}, \quad H_1 = \begin{pmatrix} 1/2 & -3/4 \\ 1/8 & -1/8 \end{pmatrix}, \tag{2.11}$$

and $H_b = 0, \forall b \notin \{-1, 0, 1\}$. Another characteristic of this type of basis is its symmetry property. It follows from [11] that the symmetric relation fulfill by these bases as

$$\phi(x) = S\phi(-x), \tag{2.12}$$

where

$$S = \begin{pmatrix} 1 & 0 \\ 0 & -1 \end{pmatrix}.$$

So, the understanding is that ϕ^1 and ϕ^2 are symmetric and antisymmetric, respectively. It is easy to confirm that

$$H_b = SH_{-b}S, \quad b \in \mathbb{Z}. \tag{2.13}$$

Relevant to the fabrication of biorthogonal wavelets, it is noteworthy that a dual scaling function $\tilde{\phi} = (\tilde{\phi}^1, \tilde{\phi}^2)$ exists, which generates another MRA as $\tilde{V}_J \subset L_2(\mathbb{R})$. Owing to the duality, the biorthogonality condition must be satisfied; namely

$$\langle \phi, \tilde{\phi}(. - b) \rangle = \delta_{0,b} I_2, \quad b \in \mathbb{Z}, \tag{2.14}$$

in which $\langle ., . \rangle$ specifies the L_2-inner product and I_2 is 2×2 identity matrix.

As mentioned above, the multiresolution spaces $\tilde{V}_J \subset L_2(\mathbb{R})$ are generated by a dual multi-generator $\tilde{\phi}$. Biorthogonality implies that the biorthogonality condition must be satisfied by the scaling sequences. In other words, the refinement masks $\tilde{H}_l, l \in \mathbb{Z}$ are obtained using (2.14) in such a way that they satisfy the following equation.

$$\sum_{l \in \mathbb{Z}} H_l \tilde{H}^T_{l+2b} = 2\delta_{0,b} I_2, \quad b \in \mathbb{Z}, \tag{2.15}$$

where the refinement masks $\tilde{H}_l, l \in \mathbb{Z}$ are provided by [11]

$$\tilde{H}_{-2} = \begin{pmatrix} -\frac{7}{64} & -\frac{5}{64} \\ \frac{87}{128} & \frac{31}{64} \end{pmatrix}, \quad \tilde{H}_{-1} = \begin{pmatrix} \frac{1}{2} & \frac{3}{16} \\ -\frac{99}{32} & -\frac{37}{32} \end{pmatrix}, \quad \tilde{H}_0 = \begin{pmatrix} \frac{39}{32} & 0 \\ 0 & \frac{15}{8} \end{pmatrix},$$
$$\tilde{H}_1 = \begin{pmatrix} \frac{1}{2} & -\frac{3}{16} \\ \frac{99}{32} & -\frac{37}{32} \end{pmatrix}, \quad \tilde{H}_2 = \begin{pmatrix} -\frac{7}{64} & \frac{5}{64} \\ -\frac{87}{128} & \frac{31}{64} \end{pmatrix},$$

and taking $l \notin -2, \ldots, 2$, we have $\tilde{H}_l = 0$.

Now, we present the set $\varphi = \{\varphi_1, \varphi_2, \ldots, \varphi_{2^{J+1}}\}$ whose elements are specified as

$$\varphi_{2b+(k-1)} := \phi^k_{J,b}, \quad \text{for} \quad k = 1, 2, \quad b \in \mathcal{J},$$

and $\varphi_1 := \sqrt{2}\phi^1_{J,0}|_{[0,1]}$, $\varphi_{2^{J+1}} := \sqrt{2}\phi^1_{J,2^J}|_{[0,1]}$. For any function $u \in L_2(\mathbb{R})$, assume that $\mathcal{P}_J$ is a projection that allows us to map u from $L_2(\mathbb{R})$ into V_J via

$$u(x) \approx \mathcal{P}_J(u)(x) = \sum_{l=1}^{2^{J+1}} c_l \varphi_l(x). \tag{2.16}$$

By using the biorthogonality condition (2.14), we can compute the coefficients $\{c_l, l = 1, \ldots, 2^{J+1}\}$ as

$$c_l = \langle u, \tilde{\varphi}_l \rangle = \int_0^1 u(x)\tilde{\varphi}_l(x)dx, \quad \text{for} \quad l = 1, \ldots, 2^{J+1}.$$

It is worthwhile to mention that there is a possibility to find the coefficients without integration via the Hermite type interpolation; namely

$$\begin{cases} c_1 := \frac{1}{\sqrt{2}}u(0), \\ c_{2l} = u(\frac{l}{2^J}), \\ c_{2l+1} = 2^{-J}u'(\frac{l}{2^J}), \quad l = 1, \ldots, 2^J - 1, \\ c_{2^{J+1}} := \frac{1}{\sqrt{2}}u(1). \end{cases} \tag{2.17}$$

To provide further simplification, we take Φ_J as a vector function, wherein the i-th element is $\varphi_i(x)$. Therefore, (2.16) can be written directly as

$$u(x) \approx C^T \Phi_J(x), \tag{2.18}$$

in which C is a vector consists of the coefficients $\{c_l, l = 1, \ldots, 2^{J+1}\}$.

Motivated by the theorem 2 in [9], one can find a bound for the error of this projection that arises from (2.16).

Theorem 2.6. *(cf [9?]) Let $u : [0, 1] \to \mathbb{R}$ is the function that belongs to the space of continuous functions with continuous derivatives up to order 4 on $[0, 1]$ ($u \in C^4[0, 1]$).*

Then $\mathcal{P}_J u$ approximates u by error bound

$$e_J(x) := |u(x) - \mathcal{P}_J(u)(x)| = \mathcal{C}\mathcal{M}_u \frac{2^{-J}}{1 - 2^{-1}},$$

where

$$\mathcal{M}_u = \max\{\max_{\xi \in [0,1]} |u^{(2)}(\xi)|, \max_{\xi \in [0,1]} |u^{(4)}(\xi)|\},$$

and $\mathcal{C}$ is a constant. Thus, it results that

$$e_J(x) = O(2^{-J}).$$

Consequently, $e_J(x)$ decays at least as quickly as 2^{-J} when J is enough large.

2.3. **Matrix representation of FI operator.** To give rise to a matrix representation for the FI of BHCSSb, defined in Subsection 2.1, it is straightforward to approximate the effect of the operator $\mathcal{I}_0^\kappa$ on the vector function $\Phi_J(x)$ via the projection $\mathcal{P}_J$ as

$$\mathcal{P}_J(\mathcal{I}_0^\kappa \Phi_J)(x) \approx I_\kappa \Phi_J(x), \tag{2.19}$$

in which I_κ is an $N \times N$ matrix where $N = 2^{J+1}$.

To proceed, for specifying the entries of I_κ, the process is started by taking the fractional integral of $\phi^k(2^J x - b)$, $k = 1, 2$, viz

$$\mathcal{I}_0^\kappa(\phi^k)(2^J x - b) = \frac{1}{\Gamma(\kappa)} \int_0^x (x-t)^{\kappa-1} \phi^k(2^J t - b)dt, \quad k = 1, 2, \quad b \in \mathcal{J}. \tag{2.20}$$

Owing to the support of $\phi^k(2^J x - b)$, the aforementioned integral can be evaluated by considering four cases.

(1) Given $b \in \mathcal{J}$, let $x \leq \frac{b-1}{2^J}$. Then, it is easy to prove that

$$\mathcal{I}_0^\kappa(\phi^k)(2^J x - b) = 0.$$

(2) Considering $x \in (\frac{b-1}{2^J}, \frac{b}{2^J})$, the integral (2.20) may be reduced to

$$a_k(x,b) := \mathcal{I}_0^\kappa(\phi^k)(2^J x - b) = \frac{1}{\Gamma(\kappa)} \int_{\frac{b-1}{2^J}}^x (x-t)^{\kappa-1} \phi^k(2^J t - b)dt, \quad \text{for} \quad k = 1, 2.$$

(3) Assume $x \in (\frac{b}{2^J}, \frac{b+1}{2^J})$ and put $b_k(x,b) := \mathcal{I}_0^\kappa(\phi^k)(2^J x - b)$ then it can be shown that

$$b_k(x,b) = \frac{1}{\Gamma(\kappa)} \left(\int_{\frac{b-1}{2^J}}^{\frac{b}{2^J}} (x-t)^{\kappa-1} \phi^k(2^J t - b)dt + \int_{\frac{b}{2^J}}^x (x-t)^{\kappa-1} \phi^k(2^J t - b)dt \right),$$

(4) If $x \geq \frac{b+1}{2^J}$ then one can write

$$\begin{aligned} c_k(x,b) := \mathcal{I}_0^\kappa(\phi^k)(2^J x - b) &= \frac{1}{\Gamma(\kappa)} \left(\int_{\frac{b-1}{2^J}}^{\frac{b}{2^J}} (x-t)^{\kappa-1} \phi^k(2^J t - b)dt \right. \\ &+ \left. \int_{\frac{b}{2^J}}^{\frac{b+1}{2^J}} (x-t)^{\kappa-1} \phi^k(2^J t - b)dt \right). \end{aligned}$$

The aforementioned integrals obtained for four cases are calculated explicitly in terms of b, κ, and J, for each value of $b \in \mathcal{J}$. We apply the Maple command "$int(f(t), t = t_1..t_2)$" to evaluate these integrals analytically. Thus, the results can be summarized as

$$T_k(x,b) := \mathcal{I}_0^\kappa(\phi^k)(2^J x - b) = \begin{cases} 0, & x \leq \frac{b-1}{2^J}, \\ a_k(x,b), & \frac{b-1}{2^J} \leq x < \frac{b}{2^J}, \\ b_k(x,b), & \frac{b}{2^J} \leq x < \frac{b+1}{2^J}, \\ c_k(x,b), & x \geq \frac{b+1}{2^J}. \end{cases} \tag{2.21}$$

To proceed, note that Equation (2.7) can be expressed as

$$\mathcal{P}_J \mathcal{I}_0^\kappa(\Phi_J)(x) = \mathcal{P}_J(\mathcal{Q}(x)) \approx I_\kappa(\Phi_J)(x), \tag{2.22}$$

where the vector function $\mathcal{Q}(x)$ has form

$$[\mathcal{Q}(x)]_{2b+(k+1)} = T_k(x,b), \quad b \in \mathcal{J}, \quad k = 1, 2, \tag{2.23}$$

with

$$[\mathcal{Q}(x)]_1 : T_1(x,0),$$
$$[\mathcal{Q}(x)]_{2^{J+1}} := T_1(x, 2^J).$$

Expanding the elements of $\mathcal{Q}(x)$ by BHCSSb enables us to find the entries of I_κ [9] as

$$I_\kappa = \begin{bmatrix} 0 & A & B_1 & \cdots & \cdots & B_{2^J-2} & Q \\ & Y & H_1 & H_2 & \cdots & H_{2^J-2} & \Theta_1 \\ & & Y & H_1 & \cdots & H_{2^J-3} & \Theta_2 \\ & & & \ddots & \ddots & \vdots & \vdots \\ & & & & Y & H_1 & \vdots \\ & & & & & Y & \Theta_{2^J-1} \\ & & & & & & M \end{bmatrix}, \tag{2.24}$$

where

$$\begin{aligned} M &= \frac{6}{\Gamma(\kappa+4)} 2^{-J\kappa}(\kappa+1), \\ Q &= \frac{1}{\Gamma(\kappa+4)} \left((1-2^{-J})^\kappa(-12(2^{3J}) + 12\kappa(2^J) + (18-6\kappa)2^{2J} - 6\kappa - 6) + 12(2^{3J})\right. \\ &\quad \left. -(18+6\kappa) \times 2^{2J} + \kappa^3 + 6\kappa^2 + 11\kappa + 6\right), \end{aligned}$$

and

$$\begin{aligned} A &= \kappa 2^{-J\kappa+\frac{1}{2}} \begin{bmatrix} \dfrac{\kappa^2+6\kappa+5}{\Gamma(\kappa+4)} & \dfrac{\kappa^2+3\kappa-4}{\Gamma(\kappa+3)} \end{bmatrix}, \\ B_{i-1} &= 2^{-J\kappa+\frac{1}{2}} \begin{bmatrix} \eta_{1,1}^{i-1} & \eta_{1,2}^{i-1} \end{bmatrix}, \qquad i = 2\ldots, 2^J-1, \end{aligned}$$

with

$$\begin{aligned} \eta_{1,1}^{i-1} &= -\frac{2^{-J\kappa+\frac{1}{2}}}{\Gamma(\kappa+4)} \left(i^\kappa(-11\kappa - 6 - 12i^3 + (6\kappa+18)i^2 - \kappa^3 - 6\kappa^2)\right. \\ &\quad \left. +(i-1)^\kappa(6\kappa + 612i^3 + (6\kappa-18)i^2 - 12\kappa i)\right), \\ \eta_{1,2}^{i-1} &= -\frac{2^{-J\kappa+\frac{1}{2}}}{\Gamma(\kappa+4)i} \left(i^\kappa(12(\kappa+3)i^3 - 6(6+\kappa^2+5\kappa)i^2 + 11\kappa^2 + 6\kappa^3 + 6\kappa + \kappa^4)\right. \\ &\quad \left. +(i-1)^\kappa(-12(\kappa+3)i^3 - 6(\kappa^2+\kappa-6) + 6(\kappa^2+3\kappa)i)\right), \end{aligned}$$

and the 2×2 block matrices

$$\begin{aligned} Y &= 2^{-J\kappa+1} \begin{bmatrix} \dfrac{3(\kappa+1)}{\Gamma(\kappa+4)} & \dfrac{3\kappa}{\Gamma(\kappa+3)} \\ -\dfrac{\kappa}{\Gamma(\kappa+4)} & -\dfrac{(\kappa-1)}{\Gamma(\kappa+3)} \end{bmatrix}, \\ H_1 &= 2^{-J\kappa+2} \begin{bmatrix} \dfrac{6(2^\kappa(\kappa-1)+1)}{\Gamma(\kappa+4)} & \dfrac{3(2^\kappa(\kappa-2)+2)}{\Gamma(\kappa+3)} \\ -\dfrac{2(\kappa+3+2^\kappa(\kappa-3))}{\Gamma(\kappa+4)} & -\dfrac{(2^\kappa(\kappa-4)+2\kappa+4)}{\Gamma(\kappa+3)} \end{bmatrix}. \end{aligned}$$

The components of the matrix $H_i = \begin{bmatrix} h_{1,1}^i & h_{1,2}^i \\ h_{2,1}^i & h_{2,2}^i \end{bmatrix}$, $i = 1, \ldots, 2^J-2$, are denoted by

$$h^i_{1,1} := -6\frac{2^{(-J\kappa)}}{\Gamma(\kappa+4)}\left((i-1)^\kappa(4-12i+2i^2-4i^3)+(i-2)^\kappa(2i^3+(\kappa-9)i^2-4(\kappa-3)i+4\kappa-4)\right.$$
$$\left.+i^{\kappa+2}(2i-(\kappa+3))\right),$$
$$h^i_{1,2} := -6\frac{2^{(-J\kappa)}}{\Gamma(\kappa+3)}\left((i-2)^\kappa(2i^2+(\kappa-6)i-2\kappa+4)+(i-1)^\kappa(4i^2+8i-4)++i^\kappa(2i^2-(\kappa+2)i)\right),$$
$$h^i_{2,1} := -\frac{2^{(J\kappa+1)}}{\Gamma(\kappa+4)}\left(i^{\kappa+2}(-3i+\kappa+3)-8i(\kappa+3)+4\kappa+12)+(i-1)^\kappa((12+4\kappa)i^2\right.$$
$$\left.+(i-2)^\kappa(3i^3-(15-\kappa)i^2-4(\kappa-6)i+4\kappa-12)\right),$$
$$h^i_{2,2} := -\frac{2^{(J\kappa+1)}}{\Gamma(\kappa+3)}\left((i-2)^\kappa(3i^2+(\kappa-10)i-2\kappa+8)-8-4\kappa+(i-1)^\kappa((8+4\kappa)i)+i^\kappa(-3i^2+(\kappa+2)i)\right).$$

The only matrix that has not been introduced yet is Θ_i, $i=1,\dots,2^J-1$ which is obtained as

$$\Theta_i = \begin{bmatrix} \mu^i_{1,1} & \mu^i_{1,2} \end{bmatrix}^T, \qquad i=1,\dots,2^J-1,$$

$$\mu^i_{1,1} := -\frac{3\sqrt{2}}{\Gamma(\kappa+4)}\left((\frac{3}{4}-\frac{1}{4}i)^\kappa(-2i^3+(\kappa+21)i^2+9\kappa+81-6(\kappa+12)i)+(1-\frac{1}{4}i)^\kappa(4i^3-48i^2+192i-256)\right.$$
$$\left.+(\frac{5}{4}-\frac{1}{4}i)^\kappa(-2i^3+(27-\kappa)i^2-10(12-\kappa)i-25\kappa+175)\right),$$
$$\mu^i_{1,2} := -\frac{\sqrt{2}}{\Gamma(\kappa+4)}\left((\frac{3}{4}-\frac{1}{4}i)^\kappa(9\kappa+108-(6\kappa+99)i+(\kappa+30)i^2-3i^3)+(1-\frac{1}{4}i)^\kappa(4(\kappa+3)i^2-32(\kappa+3)i\right.$$
$$\left.+192+64\kappa)+(\frac{5}{4}-\frac{1}{4}i)^\kappa(3i^3+(\kappa-42)i^2+(-10\kappa+195)i+25\kappa-300)\right).$$

Lemma 2.7. *Given $u\in L_2[0,1]$, assume that $u\approx \mathcal{P}_J(u) := u_J(x) = C^T\Phi_J(x)$. If $\mathcal{I}^\kappa_0(u_J)(x)$ is obtained by $C^TI_\kappa\Phi_J(x)$, Then we have*

$$\lim_{J\to\infty}\mathcal{I}^\kappa_0(u_J)(x) = \mathcal{I}^\kappa_0(u)(x). \tag{2.25}$$

Proof. Theorem 2.6 can be used to verify that

$$\lim_{J\to\infty}u_J(x) := \lim_{J\to\infty}\mathcal{P}_J(u)(x) = \lim_{J\to\infty}\sum_{l=1}^{2^{J+1}}c_l\varphi_l(x) = u(x). \tag{2.26}$$

Since the vector function $\Phi_J(x)$ consists of continuous functions, then we get

$$\lim_{J\to\infty}\int_0^x(x-t)^{\kappa-1}\sum_{l=1}^{2^{J+1}}c_l\varphi_l(t)dt = \lim_{J\to\infty}\sum_{l=1}^{2^{J+1}}c_l\int_0^x(x-t)^{\kappa-1}\varphi_l(t)dt. \tag{2.27}$$

Consequently, we have

$$\lim_{J\to\infty}\mathcal{I}^\kappa_0(u_J)(x) = \lim_{J\to\infty}C^TI_\kappa\Phi_J(x). \tag{2.28}$$

Considering Equation (2.28) and the definition 2.1 for $\kappa\in\mathbb{R}^+$, we obtain

$$\Gamma(\kappa)\mathcal{I}^\kappa_0(u)(x) = \int_0^x(x-t)^{\kappa-1}u(t)dt = \lim_{J\to\infty}\int_0^x(x-t)^{\kappa-1}u_J(t)dt = \Gamma(\kappa)\lim_{J\to\infty}C^TI_\kappa\Phi_J(x). \tag{2.29}$$

Consequently, using (2.28) and (2.29) we have

$$\lim_{J\to\infty}\mathcal{I}^\kappa_0(u_J)(x) = \mathcal{I}^\kappa_0(u)(x).$$

□

3. Method description

This section is dedicated to developing an algorithm based on the wavelet Galerkin method using the well-known BHCSSb for solving the FIDEs (1.1). One can write the operator form of the equation (1.1) as

$$({}^{C}\mathcal{D}_0^{\kappa} - c_2\mathcal{K})w = c_1 f, \tag{3.1}$$

where the operator $\mathcal{K}$ is indicated by

$$\mathcal{K}(w)(x) := \int_{\Omega} k(x,t)g(w(t))dt. \tag{3.2}$$

Proving the uniqueness of the solution of (1.1) is not hard, and considering $w(x)$ as a sufficiently smooth function, the proof can be done easy [17]. Since our proposed algorithm is based on reducing the desired equation to a Volterra-Fredholm integral equation, thus we provide the following lemma to verify the equality of the solutions.

Lemma 3.1. *(cf [17]) Assume that w, f, and k are continuous functions. The function $w(x)$ is the solution of (1.1) if, and only if, it fulfills the VFIE*

$$w(x) = \sum_{i=0}^{\eta-1} \frac{w^{(i)}(0)}{i!}x^i + c_1\mathcal{I}_0^{\kappa}(f)(x,w(x)) + c_2\mathcal{I}_0^{\kappa}\mathcal{K}(w)(x). \tag{3.3}$$

Here $\kappa \in \mathbb{R}^+$, and $\eta = -[-\kappa]$.

To implement the wavelet Galerkin method, using the operator $\mathcal{P}_J$, we can expand the unknown solution $w(x)$ based on BHCSSb, as follows.

$$w(x) \approx \mathcal{P}_J(w)(x) = W^T\Phi_J(x) := w_J(x), \tag{3.4}$$

in which W is a square matrix of order N with unknown coefficients. Putting (3.4) back into (3.3), we get

$$w_J(x) = \sum_{i=0}^{\eta-1} \frac{w^{(i)}(0)}{i!}x^i + c_1\mathcal{I}_0^{\kappa}(f)(x,w_J(x)) + c_2\mathcal{I}_0^{\kappa}\mathcal{K}(w_J)(x). \tag{3.5}$$

In the sequel, all terms are mapped into V_J using the operator $\mathcal{P}_J$.

- Putting $u_1(x) := \sum_{i=0}^{\eta-1} \frac{w^{(i)}(0)}{i!}x^i$, one can obtain

  $$u_1(x) \approx \mathcal{P}_J(u_1)(x) = U_1^T\Phi_J(x), \tag{3.6}$$

  where the l-th component of U_1 is calculated by $\langle u_1, \tilde{\varphi}_l\rangle$.
- Replacing the approximation w_J instead of w into the function $g(w(t))$ and mapping the obtained function into the space V_J, we get

  $$u_2(t) := g(w_J(t)) \approx \mathcal{P}_J(g(w_J(t))) = G^T\Phi_J(t), \tag{3.7}$$

  where l-th element of the vector G is $\langle u_2, \tilde{\varphi}_l\rangle$. A similar mapping can be done for function $k(x,t)$, viz

  $$k(x,t) \approx \mathcal{P}_J(k)(x,t) = \Phi_J^T(x)K\Phi_J(t), \tag{3.8}$$

  in which

  $$K_{i,j} = \int_0^1\int_0^1 k(x,t)\tilde{\varphi}_j(t)\tilde{\varphi}_i(x)dxdt, \quad i,j = 1,2,\ldots,N.$$

  Replacing (3.8) into $\mathcal{K}(w_J)(x)$ and using the operational matrix of product $Z_{i,j} = \langle \varphi_j, \varphi_i\rangle$, we obtain

  $$\mathcal{P}_J\mathcal{K}(w_J)(x) \approx \Phi_J^T(x)KZ\Phi_J(x) =: p_2(x) \in V_J, \tag{3.9}$$

  Note that $\mathcal{P}_J$ is a bounded projection operator, i.e.,

  $$\mathcal{P}_J(w)(x) = w(x), \quad w(x) \in V_J.$$

Equivalently, we obtain $\mathcal{P}_J^2 = \mathcal{P}_J$. According to this, the function $p_2(x)$ can be approximated by using projection operator $\mathcal{P}_J$, and then, we can summarize (3.9) as

$$\mathcal{P}_J\mathcal{K}(w_J)(x) \approx P_2^T\Phi_J(x), \tag{3.10}$$

in which P_2 is a N-dimensional vector. Using (3.10) and matrix I_κ, the Volterra-Fredholm integral $\mathcal{I}_0^\kappa\mathcal{K}(w_J)(x)$, existing in Equation (3.5), can be approximated as

$$\mathcal{I}_0^\kappa\mathcal{K}(w_J)(x) \approx P_2^T I_\kappa\Phi_J(x). \tag{3.11}$$

- Considering the above manner for the previous item, one can approximate $\mathcal{I}_0^\kappa(f)(x,w(x))$ as follows.

$$\begin{aligned}\mathcal{I}_0^\kappa(f)(x,w_J(x)) &\approx \mathcal{I}_0^\kappa(F^T\Phi_J(x))\\ &\approx F^T I_\kappa\Phi_J(x),\end{aligned} \tag{3.12}$$

in which the l-th element of N-dimensional vector F is computed by $\langle f,\tilde{\varphi}_l\rangle$.

Substituting (3.4), (3.6), (3.11), and (3.12) into (3.5) gives rise to introducing the residual

$$R(x) := \left(W^T - U_1^T - c_1F^T I_\kappa - P_2^T I_\kappa\right)\Phi_J(x) = 0. \tag{3.13}$$

Applying the Galerkin method and the biorthogonality of BHCSSb ($\langle\Phi_J,\tilde{\Phi}_J\rangle = I_N$) yields the system

$$\mathcal{F}(W) = 0, \tag{3.14}$$

with the nonlinear or linear vector function $\mathcal{F}$ of W. The generalized minimal residual method (GMRES method) [31] and Newton's method are used to determine the unknown vector W for the linear and nonlinear forms, respectively. It is worth mentioning that Newton's method is implemented with starting point $W_0 = O$(null vector) and the termination criterion is selected to be absolute residual, i.e.

$$\|\mathcal{F}(W_n)\| \le 10^{-16}, n \ge 1.$$

Assume that the linear system (3.14) has the form $AW = b$. To implement the GMRES method, we use the Matlab function "$gmres(A,b,restart,tol)$" in which "$restart$" is the number of inner iterations before restart (this scalar integer is used to control the maximum number of iterations, which in this paper has been chosen equal to 10), and "tol" is the method tolerance (use this input to control runtime and accuracy in the computing. A smaller value of tol means the answer should be more precise for the computing to be successful). tol is set to 10^{-16} in this paper.

3.1. **Convergence of the method.**

Theorem 3.2. *Consider the continuous functions g and f such that fulfill the conditions (1.3) and*

$$|f(x,w(x)) - f(x,u(x))| \le \varrho|w-u|, \tag{3.15}$$

respectively. Furthermore, one supposes that $k(x,t)$ is a sufficiently smooth function on $\Omega\times\mathbb{R}$.

If $c_1\frac{\rho M_1}{\kappa\Gamma(\kappa)} + c_2\frac{\varrho}{\Gamma(\kappa+1)} < 1$ with $\kappa\in\mathbb{R}^+$, and $M_1 := max_{x,t\in[0,1]}|k(x,t)|$, then the error of the method satisfies

$$\|w - w_J\|_\infty = O(2^{-J}). \tag{3.16}$$

Proof. Considering Lipschitz condition (1.3) and putting $M_1 = \max_{x,t\in\Omega}\{k(x,t)\}$, if the functions k and g are continuous, we can verify that

$$\begin{aligned}
\|\mathcal{I}_0^\kappa\mathcal{K}(w) - \mathcal{I}_0^\kappa\mathcal{K}(w_J)\| &= \|\mathcal{I}_0^\kappa\left(\int_\Omega k(x,t)g(w(t))dt - \int_\Omega k(x,t)g(w_J(t))dt\right)\| \\
&\le \|\mathcal{I}_0^\kappa\left(\rho\int_\Omega k(x,t)(w(t)-w_J(t))dt\right)\| \\
&\le \|\mathcal{I}_0^\kappa\left(\rho M_1\int_\Omega (w(t)-w_J(t))dt\right)\| \\
&\le \frac{M_1\rho}{\Gamma(\kappa)}\int_0^x (x-t)^{\kappa-1}\int_\Omega \|w-w_J\|dxdt \\
&\le \frac{M_1\rho}{\Gamma(\kappa)}\|w-w_J\|\int_0^x (x-t)^{\kappa-1}dt \\
&\le \frac{M_1\rho}{\kappa\Gamma(\kappa)}\|w-w_J\|. \qquad (3.17)
\end{aligned}$$

Here, Using Theorem 2.6, we have

$$\|\mathcal{I}_0^\kappa\mathcal{K}(w_J) - \mathcal{P}_J\mathcal{I}_0^\kappa\mathcal{K}(w_J)\| \le C_2M_2 2^{-J}, \qquad (3.18)$$

where $M_2 := \max\{\max_{\xi\in\Omega}|\mathcal{D}^2\mathcal{I}_0^\kappa\mathcal{K}(w_J)(\xi)|, \max_{\xi\in\Omega}|\mathcal{D}^4\mathcal{I}_0^\kappa\mathcal{K}(w_J)(\xi)|\}$. To approximate M_2, there are two situations.

(1) if $n < \eta$, then we have

$$\mathcal{D}^n\mathcal{I}_0^\kappa\mathcal{K}(w_J) = \mathcal{I}_0^{\kappa-n}\mathcal{K}(w_J), \qquad (3.19)$$

and it follows from Lemma 2.2 that

$$\begin{aligned}
\|\mathcal{D}^n\mathcal{I}_0^\kappa\mathcal{K}(w_J)\| = \|\mathcal{I}_0^{\kappa-n}\mathcal{K}(w_J)\| &\le \frac{1}{\Gamma(\kappa-n+1)}\|\mathcal{K}(w_J)\| \\
&\le \frac{M_1}{\Gamma(\kappa-n+1)}\|\int_\Omega g(w_J(t))dt\| \\
&\le \frac{M_1}{\Gamma(\kappa-n+1)}\int_\Omega \|g(w_J(t))\|dt, \qquad (3.20)
\end{aligned}$$

Consequently, the norm $\|\mathcal{D}^n\mathcal{I}_0^\kappa\mathcal{K}w_J\|$ is bounded by the continuity of function g.

(2) Let $n \ge \eta$. We refer to Lemma 2.21 [17] to show that

$$\mathcal{D}^n\mathcal{I}_0^\kappa\mathcal{K}(w_J) = {}^C\mathcal{D}^{n-\kappa C}\mathcal{D}^\kappa\mathcal{I}_0^\kappa\mathcal{K}(w_J) = {}^C\mathcal{D}^{n-\kappa}\mathcal{K}(w_J). \qquad (3.21)$$

Using Lemma 2.5, after taking the norm from both sides of (3.21), we can write

$$\begin{aligned}
\|\mathcal{D}^n\mathcal{I}_0^\kappa\mathcal{K}(w_J)\| &= \|{}^C\mathcal{D}^{n-\kappa}\mathcal{K}(w_J)\| \\
&\le \frac{1}{\Gamma(m-n+\kappa)(m-n+\kappa+1)}\|\mathcal{K}(w_J)\|, \quad (m=[n-\kappa]+1). \qquad (3.22)
\end{aligned}$$

So, for the two cases, we prove that the norm $\|\mathcal{D}^n\mathcal{I}_0^\kappa\mathcal{K}w_J\|$ is bounded.

According to the hypothesis, because $f(x,u(x))$ fulfills the Lipschitz condition (1.3), the norm of $(\mathcal{I}_0^\kappa(f)(x,w(x)) - \mathcal{I}_0^\kappa(f)(x,w_J(x)))$ can be bounded using Lemma 2.2, as follows

$$\begin{aligned}
\|\mathcal{I}_0^\kappa(f)(x,w(x)) - \mathcal{I}_0^\kappa(f)(x,w_J(x))\| &\le \varrho\|\mathcal{I}_0^\kappa(w-w_J)\| \\
&\le \frac{\varrho}{\Gamma(\kappa+1)}\|w-w_J\|. \qquad (3.23)
\end{aligned}$$

Using Theorem 2.6, one can write

$$\|\mathcal{I}_0^\kappa(f)(x,w_J) - \mathcal{P}_J\mathcal{I}_0^\kappa(f)(x,w_J)\| \le C_3M_3 2^{-J}, \qquad (3.24)$$

where

$$M_3 := \max\{\max_{\xi\in[0,1]} |\mathcal{D}^2\mathcal{I}_0^\kappa f(\xi, w_J(\xi))|, \max_{\xi\in[0,1]} |\mathcal{D}^4\mathcal{I}_0^\kappa f(\xi, w_J(\xi))|\}.$$

To evaluate the approximate value of M_3, we follow the two cases that we investigated for M_2. But, we ignore the evaluation of it due to the simplicity and similarity to M_2.

Subtracting (3.3) from

$$w_J(x) = \mathcal{P}_J(p_1)(x) + c_1\mathcal{P}_J(\mathcal{I}_0^\kappa)(f)(x, w_J(x)) + c_2\mathcal{P}_J(\mathcal{I}_0^\kappa)(\mathcal{K})(w_J)(x), \tag{3.25}$$

we have

$$\begin{aligned} w(x) - w_J(x) = {} & p_1 - \mathcal{P}_J(p_1) + c_1\mathcal{I}_0^\kappa(f)(x, w(x)) - c_1\mathcal{P}_J\mathcal{I}_0^\kappa(f)(x, w_J(x)) + c_2\mathcal{I}_0^\kappa\mathcal{K}(w)(x) \\ & - c_2\mathcal{P}_J\mathcal{I}_0^\kappa\mathcal{K}(w_J)(x) + c_1\mathcal{I}_0^\kappa(f)(x, w_J(x)) - c_1\mathcal{I}_0^\kappa(f)(x, w_J(x)) \\ & + c_2\mathcal{I}_0^\kappa\mathcal{K}(w_J)(x) - c_2\mathcal{I}_0^\kappa\mathcal{K}(w_J)(x), \end{aligned} \tag{3.26}$$

where $u_1(x) := \sum_{i=0}^{n-1} \frac{w^{(i)}(0)}{i!}x^i$. After taking the norm from both sides of (3.26), we employ Equations (3.17), (3.18), (3.23), (3.24) and apply the triangle inequality to indicate that

$$\begin{aligned} \|w - w_J\| \leq {} & \|u_1 - \mathcal{P}_J(u_1)\| + c_1\|\mathcal{I}_0^\kappa(f)(x, w(x)) - \mathcal{I}_0^\kappa(f)(x, w_J(x))\| \\ & + c_1\|\mathcal{I}_0^\kappa(f)(x, w_J(x)) - c_1\mathcal{P}_J\mathcal{I}_0^\kappa(f)(x, w_J(x))\| \\ & + c_2\|\mathcal{I}_0^\kappa\mathcal{K}(w)(x) - \mathcal{I}_0^\kappa\mathcal{K}(w_J)(x)\| \\ & + c_2\|\mathcal{I}_0^\kappa\mathcal{K}(w_J)(x) - \mathcal{P}_J(\mathcal{I}_0^\kappa)\mathcal{K}(w_J)(x)\| \\ & \leq C_4M_4 2^{-J} + c_1\frac{\rho M_1}{\kappa\Gamma(\kappa)}\|w - w_J\| + c_1C_2M_2 2^{-J} \\ & + c_2\frac{\varrho}{\Gamma(\kappa+1)}\|w - w_J\| + c_2C_3M_3 2^{-J} \\ & = \left(c_1\frac{\rho M_1}{\kappa\Gamma(\kappa)} + c_2\frac{\varrho}{\Gamma(\kappa+1)}\right)\|w - w_J\| + \left(C_4M_4 + c_1C_2M_2 + c_2C_3M_3\right)2^{-J}, \end{aligned} \tag{3.27}$$

where $\|u_1 - \mathcal{P}_J(u_1)\| \leq C_4M_4 2^{-J}$ with

$$M_4 := \max\{\max_{\xi\in[0,1]} |\mathcal{D}^2u_1(\xi)|, \max_{\xi\in[0,1]} |\mathcal{D}^4u_1(\xi)|\}$$

By putting $\lambda := c_1\frac{\rho M_1}{\kappa\Gamma(\kappa)} + c_2\frac{\varrho}{\Gamma(\kappa+1)}$, if $\lambda < 1$, then we obtain

$$\|w(x) - w_J(x)\| \leq \frac{C}{1-\lambda}2^{-J}, \tag{3.28}$$

where $C := C_4M_4 + c_1C_2M_2 + c_2C_3M_3$.

□

4. Numerical Experiments

To give a demonstration of the accuracy and efficiency of the presented algorithm, some illustrative examples are provided in this section. To this end, some error criteria are used so that we introduce them as follows.

- The L_∞-error is obtained by

  $$\|w(x) - w_J(x)\|_\infty = \sup\{|w(x) - w_J(x)| : x \in [0,1]\}.$$

- The L_2-error is calculated by

  $$\|w(x) - w_J(x)\|_2 = \left(\int_0^1 |w(x) - w_J(x)|^2 dx\right)^{1/2}.$$

TABLE 1. The obtained L_2-error due to the increase of the parameter J and compare the results with Alpert's multiwavelets method for Example 4.1.

	Presented method			[27]
	$J=3$	$J=4$	$J=5$	$r=3, J=5$
L_2-error	3.5325×10^{-3}	1.5752×10^{-3}	7.0524×10^{-4}	1.4297×10^{-3}
	$J=6$	$J=7$	$J=8$	
L_2-error	3.2012×10^{-4}	1.4912×10^{-4}	6.9567×10^{-5}	

TABLE 2. The L_∞-error for Example 4.1.

x	0.1	0.3	0.5	0.7	0.9
J=3	2.74×10^{-3}	4.30×10^{-3}	3.13×10^{-3}	2.66×10^{-3}	2.05×10^{-3}
J=4	2.07×10^{-3}	1.67×10^{-3}	1.43×10^{-3}	1.19×10^{-3}	9.04×10^{-3}
J=5	1.02×10^{-3}	7.90×10^{-4}	7.62×10^{-4}	5.70×10^{-4}	4.50×10^{-4}
x	0.91	0.93	0.95	0.97	0.99
J=3	2.02×10^{-3}	1.96×10^{-3}	1.89×10^{-3}	1.83×10^{-3}	1.76×10^{-3}
J=4	8.96×10^{-4}	8.77×10^{-4}	8.41×10^{-4}	8.11×10^{-4}	7.84×10^{-4}
J=5	4.11×10^{-4}	3.77×10^{-4}	3.90×10^{-4}	3.36×10^{-4}	3.77×10^{-4}

- Root Mean Square Error (RMSE) is used to demonstrate the standard deviation of the residuals and is determined as

$$RMSE=\left(\frac{1}{N}\sum_{i=1}^{N}|w(x_i)-w_J(x_i)|^2\right)^{1/2},$$

in which N is sample size and $x_i := i/N$.

According to our analysis, the rate of convergence is equal to $O(2^{-J})$. Thus, our expectation is that when the refinement parameter increases from J to $J+1$, the error is approximately halved, and the rate of convergence is approximately 1, viz

$$\log_2\frac{u-u_{J+1}}{u-u_J}\approx\log_2\frac{2^{J+1}}{2^J}=1.$$

To verify our analysis, in all the following examples, we will try to demonstrate that increasing the refinement parameter from J to $J+1$, results in the error being approximately halved, and the rate of convergence is approximately 1.

Example 4.1. The first example is dedicated to the FIDEs [27]

$${}^{C}\mathcal{D}_0^{5/6}w(x)+\int_0^1 xe^t(w(t))^2dt=\frac{3}{\Gamma(1/6)}\left(2\sqrt[6]{x}-\frac{432}{91}\sqrt[6]{x^{13}}\right)+x(674-248e),$$

with condition $w(0)=0$. Motivated by reference [27], the exact solution is indicated by $w(x)=x-x^3$.

We report Table 1 to demonstrate when the parameter J increases, the error reduces. By choosing the same J, one can observe that our algorithm gives results better than the ones obtained by Alpert's multiwavelets method. The L_∞-error is tabulated in Table 2 by taking different values for x and J. Figure 1 demonstrates the approximate solution and L_∞-error taking $J=5$.

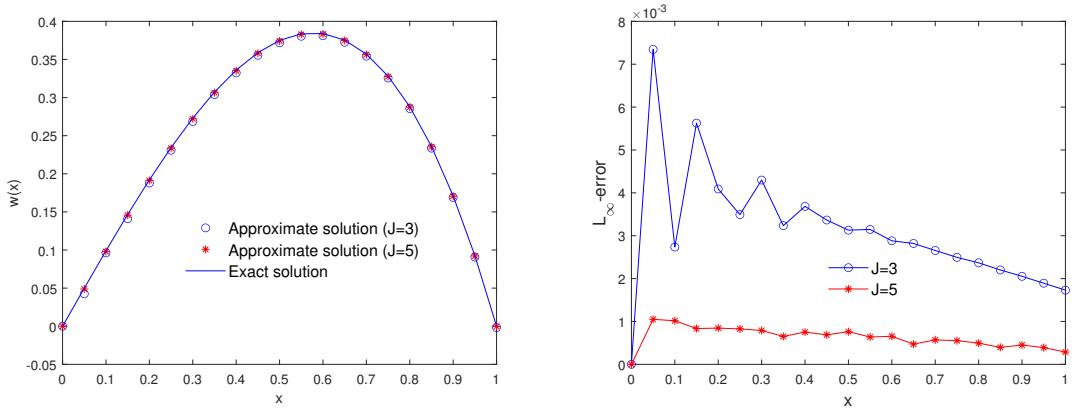

FIGURE 1. Plots of the obtained estimated solution and corresponding L_∞-error for Example 4.1.

TABLE 3. The obtained L_2-error due to the increase of the parameter J and compare the results with Alpert's multiwavelets method for Example 4.2.

	Proposed method			Alpert's multiwavelets method [27]
	$J=2$	$J=3$	$J=4$	$r=3, J=5$
L_2-error	1.8185×10^{-3}	6.7717×10^{-4}	2.5194×10^{-4}	4.1661×10^{-4}
	$J=5$	$J=6$	$J=7$	
L_2-error	1.0069×10^{-4}	4.0435×10^{-5}	1.7794×10^{-5}	

Example 4.2. Consider the nonlinear FIDEs [27]

$$ {}^{C}\mathcal{D}_0^{1/2}w(x)+\int_0^1 xt(w(t))^4dt=\frac{1}{\Gamma(1/2)}\left(8/3x^{3/2}-2x^{1/2}\right)-\frac{x}{1260},\qquad x\in[0,1], $$

with

$$ w(0)=0. $$

The exact solution is reported as $u(x)=x^2-x$ in [27].

In Table 3, the efficacy of parameter J and its effect on L_2-error are illustrated, and a comparison between the presented method and Alpert's multiwavelets method is reported. For more illustration, Figure 2 is plotted to indicate the effect of J. Figure 3 demonstrates the approximate solution when the parameter J is changed and provides a good view of accuracy. Due to the good accuracy of the presented method, the plots of the solutions are very close to each other and close to the exact solution.

Example 4.3. In this example, we concentrate on the nonlinear FIDEs

$$ {}^{C}\mathcal{D}_0^{\kappa}u(x)+3x^2u^4(x)-\int_0^1 x^2(t+1)w^2(t)dt=\frac{18x^4\Gamma\left(\frac{3}{2}-\kappa\right)-5x^2\Gamma\left(\frac{3}{2}-\kappa\right)+3\sqrt{\pi}x^{1/2-\kappa}}{6\Gamma(\frac{3}{2}-\kappa)}, $$

in which $0<\kappa\leq1$. The exact solution is $w(x)=\sqrt{x}$.

Table 4 shows the L_2-error, RMSE, and the order of convergence, where the value of J changes. What is important is that, in any practically relevant application, we know that one cannot expect the exact solution to have a continuous derivative near the origin. Therefore, when the exact solution does not have a continuous derivative near the origin, the numerical solution does not approach the exact solution with the use of other bases. To overcome this issue and

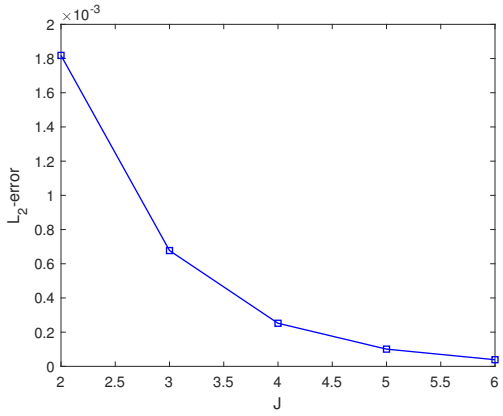

FIGURE 2. The reduction in L_2-error corresponding to the increase of J for Example 4.2.

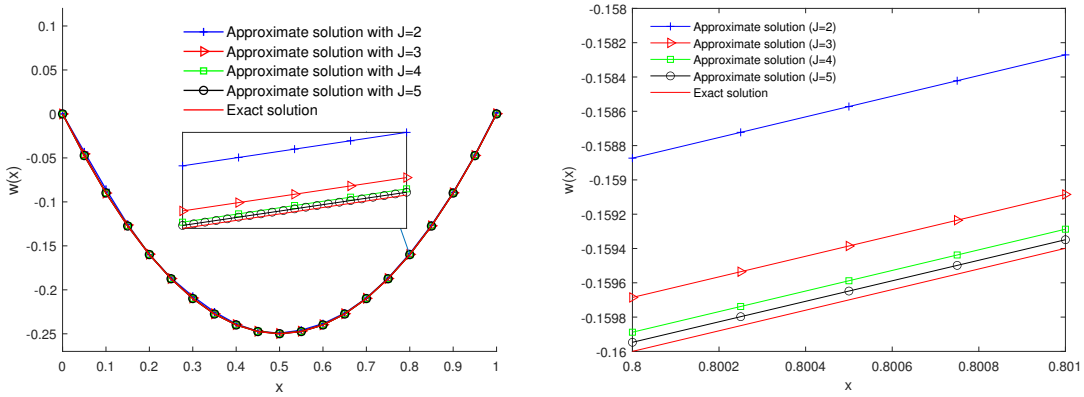

FIGURE 3. Plots of the approximate solution and a zoom of inner sub-figure of Example 4.2, taking different values for J.

TABLE 4. The obtained L_2-error and RMSE under the effect of J for Example 4.3.

J	2	3	4	5	6
RMSE	1.3133×10^{-2}	7.3342×10^{-3}	4.0678×10^{-3}	2.2394×10^{-3}	1.3234×10^{-3}
L_2-error	2.0705×10^{-2}	1.1056×10^{-2}	5.8400×10^{-3}	3.0775×10^{-3}	1.6153×10^{-3}
order	–	0.90512	0.92083	0.92418	0.93002

obtain a higher-accuracy numerical solution, we can increase the refinement level J when we use the BHCSSb. This is applicable based on the multi-scale property of wavelet systems.

Figure 4 plotted to elucidate what is the effect of refinement level J. According to Figures 4 and 5, it is worth mentioning that the obtained numerical solution is convergent to the exact one, and convergence occurs even in the vicinity of the origin.

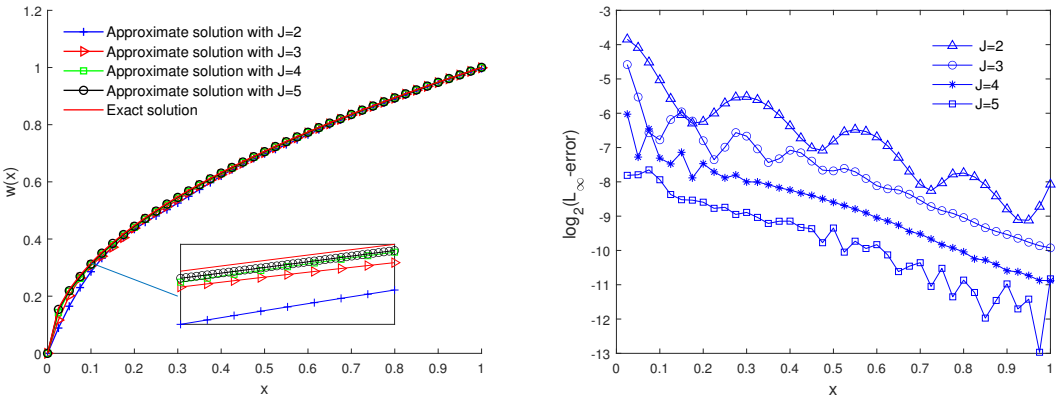

FIGURE 4. Plots of the obtained numerical solution and corresponding L_∞-error for Example 4.3.

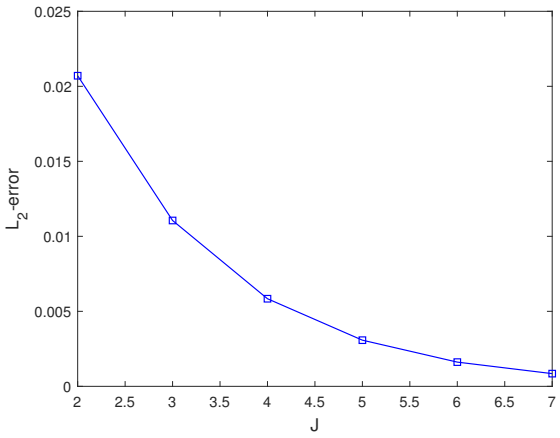

FIGURE 5. The reduction in L_2-error corresponding to the increase of J for Example 4.3.

Example 4.4. We devote the fourth example to the linear equation

$$ {}^{C}\mathcal{D}_0^{\kappa} w(x) - \int_0^1 xtw(t)dt = 3x^2 - \frac{x}{5}, $$

with $w(0) = 0$. The exact solution for this equation in the case of $\kappa = 1$ is $w(x) = x^3$. Figure 6 the numerical solution for $J = 4$ and various $0 < \kappa \leq 1$. We know that as $\kappa \to 1$, the numerical solution should be tend to $w(x) = x^3$. The L_2-error, RMSE, and condition number of the coefficient matrix (3.14) are reported in Table 5 by taking $\kappa = 1$.

Example 4.5. For the last one, let us consider the linear FIDE

$$ {}^{C}\mathcal{D}_0^{0.5} w(x) - \int_\Omega (x+t)w(t)dt = f(x), $$

such that $w(0) = 0$ and

$$ f(x) = \sqrt{2}\,\mathrm{S}\left(\frac{\sqrt{2x}}{\sqrt{\pi}}\right)\sin(x) + \sqrt{2}\,\mathrm{C}\left(\frac{\sqrt{2x}}{\sqrt{\pi}}\right)\cos(x) + \cos(1)\,x - \sin(1) + \cos(1) - x, $$

TABLE 5. The effect of the parameter J on L_2-error, RMSE, and condition number, taking $\kappa = 1$, for Example 4.4.

J	3	4	5	6	7
RMSE	2.2821×10^{-6}	1.1803×10^{-6}	6.0204×10^{-7}	3.1747×10^{-7}	1.6081×10^{-7}
L_2-error	1.6147×10^{-6}	8.3508×10^{-7}	4.2596×10^{-7}	2.2461×10^{-7}	1.1378×10^{-7}
order	–	0.95125	0.97120	0.97325	0.98125
Condition number	1.55019	1.57914	2.01282	2.06217	2.15241

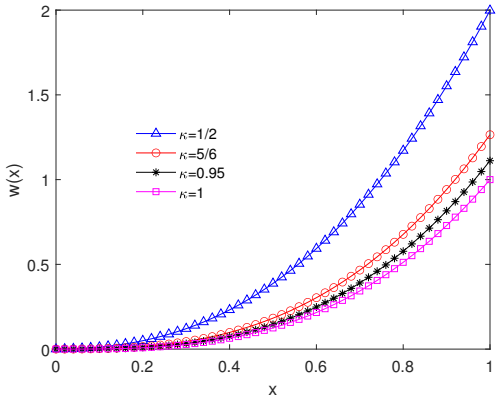

FIGURE 6. The obtained numerical solution of Example 4.4, taking $J = 4$ and various κ.

TABLE 6. The effect of the parameter J on L_2-error, RMSE, and condition number for Example 4.5.

J	3	4	5	6	7
RMSE	1.9756×10^{-3}	7.0627×10^{-4}	2.7144×10^{-4}	1.2876×10^{-4}	3.0192×10^{-5}
L_2-error	1.9405×10^{-3}	7.0444×10^{-4}	2.8009×10^{-4}	1.4215×10^{-4}	6.0484×10^{-5}
order	–	1.461867	1.330585	1.215453	1.090101
Condition number	15.042517	15.190189	15.728786	15.952871	16.152359

in which the Fresnel integrals $\mathcal{S}(x)$ and $\mathcal{C}(x)$ are indicated by

$$\mathcal{C}(x) = \sum_{i=0}^{\infty} (-1)^i \frac{x^{4i+3}}{(2i+1)!(4i+3)},$$

and

$$\mathcal{S}(x) = \sum_{i=0}^{\infty} (-1)^i \frac{x^{4i+1}}{(2i)!(4i+1)}.$$

The solution of this example is $w(x) = \sin(x)$.

Table 6 is reported to display the effect of parameter J on the L_2-error, RMSE, order of convergence and condition number. Tables 5 and 6 confirm our analysis in the previous section about convergence.

5. CONCLUSION

In the present method, to obtain the numerical solution of FIDEs, these problems must first be reduced to a Volterra-Fredholm integral equation (VFIE) with a weakly singular kernel. Then, the wavelet Galerkin method is applied to

estimate the numerical behavior of the VFIE. To this end, a matrix representation of the fractional integral based on BHCSSb is presented, and we use it to reduce the problem to a system of algebraic equations. The combination of singularity and the challenge related to nonlinearity poses a formidable obstacle in solving the desired equations, but our method overcomes them well. Method convergence is proved, and our investigation verifies that the convergence rate is $O(2^{-J})$ where $J \in \mathbb{Z}^+ \cup \{0\}$ is the refinement level. The numerical examples confirm our theoretical analysis. The results illustratively show the efficiency and accuracy of the method, and a comparison between the present method and others demonstrates the accuracy and effectiveness of the method.

References

[1] B. Alpert, G. Beylkin, R. R. Coifman, and V. Rokhlin, *Wavelet-like bases for the fast solution of second-kind integral equations*, SIAM J. Sci. Statist. Comput., *14*(1) (1993), 159–184.

[2] H. Aminikhah, *A new analytical method for solving systems of linear integro-differential equations*, J. King Saud Univer. Sci., *23*(4) (2011), 349–353.

[3] C. N. Angstmann, B. I. Henry, and A. V. McGann, *A fractional order recovery SIR model from a stochastic process*, Bull. Math. Biol., *78*(3) (2016), 468–499.

[4] A. Arikoglu and I. Ozkol, *Solution of fractional integro-differential equations by using fractional differential transform method*, Chaos, Solitons & Fractals, *40* (2009), 521–529.

[5] M. Asadzadeh and B. N. Saray, *On a multiwavelet spectral element method for integral equation of a generalized Cauchy problem*, BIT Numerical Mathematics, *62* (2022), 383-–1416.

[6] M. S. Asl, M. Javidi, and Y. Yan, *A novel high-order algorithm for the numerical estimation of fractional differential equations*, J. Comput. Appl. Math., *342* (2018), 180–201.

[7] R. L. Bagley and P. J. Torvik, *Fractional Calculus in the Transient Analysis of Viscoelastically Damped Structures*, AIAA. J., *23*(6) (1985), 918–925.

[8] R. T. Baillie, *Long Memory Processes and Fractional Integration in Econometrics*, J. Econometrics, *73*(1) (1996), 5–59.

[9] H. Bin Jebreen and I. Dassios, *A Biorthogonal Hermite Cubic Spline Galerkin Method for Solving Fractional Riccati Equation*, Mathematics, *10*(9) (2022), 1461.

[10] V. Daftardar-Gejji, Y. Sukale, and S. Bhalekar, *A new predictorcorrector method for fractional differential equations*, Appl. Math. Comput., *244* (2014), 158–182.

[11] W. Dahmen, B. Han, R.Q. Jia, and A. Kunoth, *Biorthogonal multiwavelets on the interval: Cubic Hermite splines*, Constr. Approx., *16* (2000), 221–259.

[12] K. Diethelm, *The analysis of fractional differential equations, An Application-Oriented Exposition Using Differential Operators of Caputo Type*, Springer-Verlag Berlin Heidelberg, 2010.

[13] K. Diethelm, N. Ford, and A. Freed, *Detailed error analysis for a fractional Adams method*, Numer. Algorithms, *36*(1) (2004), 31–52.

[14] M. R. Eslahchi, M. Dehghan, and M. Parvizi, *Application of the collocation method for solving nonlinear fractional integro-differential equations*, J. Comput. Appl. Math., *257* (2014), 105–128.

[15] J. H. He, *Nonlinear Oscillation with Fractional Derivative and its Applications*, Interna-tional Conference on Vibrating Engineering , (1998), 288–291.

[16] J. H. He, *Some Applications of Nonlinear Fractional Differential Equations and Their Approximations*, Bull. Sci. Technol., *2* (1999), 86–90.

[17] A. Kilbas, H. M. Srivastava, and J. J. Trujillo, *Theory and applications of fractional differential equations*, 24. Elsevier B. V., Amsterdam, 2006.

[18] X. Li, *Numerical solution of fractional differential equations using cubic B-spline wavelet collocation method*, Commun. Nonlinear Sci. Numer. Simulat., *17*(10) (2012), 3934–3946.

[19] F. Mainardi, *Fractional Calculus: Some Basic Problems in Continuum and Statistical Mechanics. Fractals and Fractional Calculus in Continuum Mechanics*, New York, Springer Verlag, 1997.

[20] B. Mandelbrot, *Some Noises with* $1/f$ *Spectrum, a Bridge between direct Current and White Noise*, IEEE Trans Inform Theory, *2* (1967), 289–298.

[21] M. Meerschaert and C. Tadjeran, *Finite Difference Approximations for Two-Sided Space-Fractional Partial Differential Equations*, Appl. Numer. Math., *56*(1) (2006), 80–90.
[22] E. M. Mendes, G. H. Salgado, and L. A. Aguirre, *Numerical solution of caputo fractional differential equations with infinity memory effect at initial condition*, Commun. Nonlinear Sci. Numer. Simulat., *69* (2019), 237–247.
[23] R. Metzler and J. Klafter, *The Restaurant at the End of the Random Walk: Recent Developments in the Description of Anomalous Transport by Fractional Dynamics*, Journal of Physics A: Mathematical and General, *37* (2004), 161–208.
[24] S. Momani and K. Al-Khaled, *Numerical Solutions for Systems of Fractional Differential Equations by the Decomposition Method*, Appl. Math. Comput., *162*(3) (2005), 1351–1365.
[25] S. Momani and M. A. Noor, *Numerical methods for fourth order fractional integro-differential equations*, Appl. Math. Comput., *182* (2006), 754–760.
[26] S. Momani and A. Qaralleh, *An Efficient Method for Solving Systems of Fractional Integro-Differential Equations*, Comput. Math. Appl., *52* (2006), 459–470.
[27] S. Paseban-Hag, E. Osgooei, and E. Ashpazzadeh, *Alpert wavelet system for solving fractional nonlinear Fredholm integro-differential equations*, Comput. Methods Differ. Equ., *9*(3) (2021), 762–773.
[28] P. Rahimkhani, Y. Ordokhani, and E. Babolian, *A New Operational Matrix based on Bernoulli Wavelets for Solving Fractional Delay Differential Equations*, Numer. Algorithms., *74* (2017), 223–245.
[29] E. A. Rawashdeh, *Numerical solution of fractional integro-differential equations by collocation method*, Appl. Math. Comput., *176* (2006), 1–6.
[30] Y. A. Rossikhin and M. V. Shitikova, *Applications of Fractional Calculus to Dynamic Problems of Linear and Nonlinear Hereditary Mechanics of Solids*, Appl. Mech. Rev., *50*(1) (1997), 15–67.
[31] Y. Saad and M. H. Schultz, *GMRES: A generalized minimal residual method for solving nonsymmetric linear systems*, SIAM J. Sci. Stat. Comput., *7* (1986), 856–869.
[32] H. Saeedi, M. Mohseni Moghadam, N. Mollahasani, and G. N. Chuev, *A CAS wavelet method for solving nonlinear Fredholm integro-differential equations of fractional order* , Commun. Nonl. Sci. Numer. Simul., *16* (2011), 1154–1163.
[33] P. K. Sahu and S. S. Ray, *A numerical approach for solving nonlinear fractional VolterraFredholm integro-differential equations with mixed boundary conditions*, Int. J. Wavelets Multi., *14*(5) (2016), 1650036.
[34] G. H. O. Salgado and L. A. Aguirre, *A hybrid algorithm for Caputo fractional differential equations*, Commun. Nonlinear Sci. Numer. Simulat., *33* (2016), 133–140.
[35] B. N. Saray, *Abel's integral operator: sparse representation based on multiwavelets*, BIT Numerical Mathematics, *61* (2021), 587–606.
[36] B. N. Saray, *An effcient algorithm for solving Volterra integro-differential equations based on Alpert's multiwavelets Galerkin method*, J. Comput. Appl. Math., *348* (2019), 453-465.
[37] Y. Yan, K. Pal, and N. Ford, *Higher order numerical methods for solving fractional differential equations*, BIT Numerical Mathematics, *54* (2014) 555–584.
[38] L. Zhu and Q. Fan, *Solving fractional nonlinear Fredholm integro-differential equations by the second kind Chebyshev wavelet*, Commun. Nonlinear Sci. Numer. Simulat., *17* (2012), 2333–2341.